ORIGINAL ARTICLE

Journal Section

Indoor Wideband Directional Millimeter Wave Channel Measurements and Analysis at 26 GHz, 32 GHz, and 39 GHz

Mohsen Khalily[1] | **Sohail Taheri**[1] | **Sohail Payami**[1] | **Mir Ghoraishi**[1] | **Rahim Tafazolli**[1]

[1]Institute for Communication Systems (ICS), home of the 5G Innovation Centre (5GIC) Department of Electronic Engineering, University of Surrey, Guildford, Surrey, GU2 7XH, U.K

Correspondence
Mohsen Khalily, Institute for Communication Systems (ICS), home of the 5G Innovation Centre (5GIC) Department of Electronic Engineering, University of Surrey, Guildford, Surrey, GU2 7XH, U.K
Email: m.khalily@surrey.ac.uk

Funding information
This project is supported by a grant from 5GIC, University of Surrey, U.K.

This paper presents details of the wideband directional propagation measurements of millimetre-wave (mmWave) channels in the 26 GHz, 32 GHz, and 39 GHz frequency bands in an indoor typical office environment. More than 14400 power delay profiles (PDPs) were measured across the 26 GHz band and over 9000 PDPs have been recorded for the 32 GHz and 39 GHz bands at each measurement point. A mmWave wideband channel sounder has been used, where signal analyzer and vector signal generator was employed. Measurements have been conducted for both co- and cross-antenna polarization. The setup provided 2 GHz bandwidth and the mechanically steerable directional horn antenna with 8 degrees beamwidth provides 8 degrees of directional resolution over the azimuth for 32 GHz and 39 GHz while 26 GHz measurement setup provides the angular resolution of 5 degrees. Measurements provide path loss, delay and spatial spread of the channel. Large-scale fading characteristics, RMS delay spread, RMS angular spread, angular and delay dispersion are presented for three mmWave bands for the line-of-sight (LoS) scenario.

Abbreviations: LoS, line of sight; mmWave, millimetre wave; PL, path loss; AOA, angle of arrival; RX, receiver; TX, transmitter; LSF, large-scale-fading; RMS delay spread, root mean square delay spread; RMS angular spread, root mean square angular spread.

KEYWORDS
millimetre wave channel propagation, 26 GHz, 32 GHz, 39 GHz, indoor, 5G, large scale fading, RMS delay spread, RMS angular spread, path loss.

1 | INTRODUCTION

Fifth generation (5G) mobile network is expected to emerge for initial deployment from 2020 onwards to overcome high data traffic and ever-increasing demand for higher transmission speed. Furthermore, to develop 5G systems with higher bandwidth and low latency, researchers and industries are becoming more and more interested to study millimetre wave (mmWave) frequency bands for small cell operations in dense urban environments, and mounting demand in using mmWave bands for indoor and outdoor 5G wireless communication as microwave wireless spectrum (spectrum below 6 GHz) is almost occupied for different applications and not enough to meet future needs. While mmWave spectrum bands offer an excessive chance to increase the channel capacity, little information is accessible about the channel propagation at these new carrier frequencies. Such characterization of the wireless channels is particular crucial to the deployment of mmWave MIMO systems where the use of beamforming techniques is inevitable, [25, 28, 27] and references therein.

Additionally, propagation measurements in indoor and outdoor environments at mmWave frequency bands are required to produce statistical channel models to support the development of new standards and technologies for future 5G wireless communication systems. Moreover, fundamental knowledge of the mmWave channel propagation characteristics to predict signal strength and multipath time delays are vital to conducting 5G system design precisely. By considering these, and the fact that different scenarios are considered for mmWave deployment, necessitate the need for new channel models at mmWave frequencies for different scenarios and environment. Recently, to fill this research gap, several indoor and outdoor channel measurement campaigns have been performed at different mmWave frequency bands [33, 29, 32, 40, 36].

For example, mmWave channel measurements at 81 GHz band (81-86 GHz) over 5 GHz of bandwidth for point-to-point communications in a long street canyon environment have been performed in Helsinki, Finland [18]. The results demonstrate that although LoS component is dominant but also multipath exist in this band. Moreover, several mmWave channel measurement campaigns for the 28 GHz band have been conducted and path loss (PL), root mean square (RMS) delay spread, and multipath effects have been studied. For instance, measurements presented in [5] showed that higher transmitter (TX) antenna can increase the coverage compared to the TX with the lower antenna heights, due to fewer obstructions. Multipath delay spreads, number of multipath components and large-scale PL have been studied by New York University (NYU) wireless research centre at 28 GHz, 38 GHz, and 73 GHz for both access and backhaul scenario and the first 3-D measurement-based mmWave wideband statistical channel impulse model for 28 GHz propagation is presented [31].

Polarimetric and wideband directional channel measurement has been performed at 32 GHz and 39 GHz and presented in [12]. RMS delay spread and power angular spectrum have been discussed for different polarization configuration. RMS delay spread at different polarizations show small difference which can be due to specific scatterers in the channel. 3GPP path loss has been studied in [11] where directional path loss at three different frequency bands; 26 GHz, 32 GHz, and 39 GHz have been measured in outdoor environment with different base station height.

While many mmWave channel measurements have been conducted for the 60 GHz indoor environment [38, 2, 42, 7, 35] there are also several indoor measurement campaigns on other mmWave bands which don't suffer high

oxygen absorption loss, unlike 60 GHz.

Recently, radio propagation transmission characteristics of 28 GHz mm wave band in building and urban cellular systems are presented in [16]. The channel parameters of mmWave are presented for micro-cell in urban and indoor NLoS scenario. The measurements were performed in South Korea and the multipath channel, power delay profile and power angular spectrum have been studied. In [20] the wideband mmWave channel propagation characteristics with both directional and omnidirectional antennas in the indoor environment at 28 GHz is presented. The path loss models, received power and root mean square (RMS) delay spreads parameters are analysed and discussed.

In [30], propagation measurements at 2.9 GHz, 29 GHz and 61 GHz carrier frequencies in indoor office, shopping mall, and outdoor scenario have been conducted. The blockage and material penetration losses of mmWave frequencies have been presented. Also the experimental prototype system is described at 28 GHz where it maintains high data rates on both the downlink and uplink in outdoor and indoor scenarios. In [21] indoor mmWave channel measurement at 28 GHz and 73 GHz have been conducted. The measurements employed rotatable directional horn antennas where directional and omni-directional path loss models and directional multipath RMS delay spread have been reported. Reflection and penetration loss measurement at 28 GHz is performed and a large penetration loss of 45 dB through an office building is presented in [39].

In [1], mmWave indoor propagation characteristics including multipath delay spread values and path loss models using omnidirectional and directional antennas are discussed. The performance of the four 5G candidate frequency bands; 28 GHz, 39 GHz, 60 GHz and 73 GHz, are investigated in LoS and NLoS scenarios using real time frequency measurements conducted in indoor environments. It has been noted that concrete walls and wood have a much more serious effect on signals than plaster board walls and glass. The delay spread, number of the received multipath and received power are decreased in NLoS environment due to high path loss in NLoS scenario compared to LoS rays. Also, LoS and NLoS scenarios have been studied at 26 GHz in [13].

In [9] wideband mmWave measurement campaigns in the 60 GHz and 70 GHz bands have been conducted over 5 GHz bandwidth. Measurements have been performed by using vector network analyser (VNA) in the different type of indoor environment such as shopping malls, railway stations, and office environment. Zhu et al. performed indoor mmWave channel measurement and presented path loss component and shadowing fading at 45 GHz using the different type of antennas [41]. Measurements have been conducted in the conference room, cubic office, and living room for LoS and none line of sight(NLoS)scenarios. Another mmWave channel measurement has been conducted at 28 GHz band in an indoor laboratory [37]. Measurements have been performed by using rotatable horn antennas that scan the whole azimuth plane using VNA channel sounding method.

In [15], CI and FI path loss models are compared using measurement data in the 28 GHz and 38 GHz bands for indoor office scenario. In [34] path loss in different floors in an indoor environment is measured for different frequency bands between 0.8 and 37 GHz.

In [19] the path loss model is investigated based on measurement results collected in a railway and an airport passenger terminal. With a steerable directional antenna, the path loss dependency is analysed in terms of bore-sight angle orientation as well as transmitter - receiver separation distance. Directional RMS delay spread is presented in [14] for indoor propagation channel using highly directional steerable horn antennas at 28 GHz.

[17] presents an indoor study in Qualcomm building, NJ, USA with comparative study of the 2.9 GHz and 29 GHz bands. In addition, measurements have been performed with omnidirectional and directional antennas. The path loss, excess delay, RMS delay and power delay profile of the received paths are discussed. The measurements results are indicated that 29 GHz is very sensitive in terms of loss and delay.

In [3] an integrated 38 GHz 5G mmWave radio access experiment platform is presented to adopt the hybrid beamforming architecture with phased array antenna. In indoor scenario, this platform achieves more than 1 Gbps data

rate over 100 m transmission range.

Aside of universities and research institutes, a number of projects on mmWave channel models have been also conducted by industry as well, such as METIS [23], mmMAGIC [22], and MiWEBA [24] for different scenarios and frequency bands in indoor and outdoor environments.

There are several mmWave frequency bands of interest for 5G wireless network. A short history of the 5G pioneer bands is presented in [10]. Also, Ofcom proposed 26 GHz band as a pioneer band for 5G in Europe and also highlighted 32 GHz and 40 GHz as promising bands for 5G in the UK [26]. Additionally, 39 GHz is recommended by FCC for 5G deployment in the US [6].

This paper aims to get a detailed insight into large-scale fading (LSF) characteristics, angular and delay spread for the mmWave frequency bands at 26 GHz, 32 GHz, and 39 GHz for co- and cross- polarization antenna configurations over 2 GHz bandwidth. For this purpose, a large amount of measurements have been conducted in the office environment. The ultimate purpose of this measurement campaign is to acquire a reliable set of data with appropriate resolution to propose a wideband, directional channel model for 5G indoor small cell scenarios at 26 GHz, 32 GHz and 39 GHz. RMS delay spreads of channel, power angular spectrum, path loss exponent, and standard deviation of shadow fading have been studied and details of measurement description, parameters as well as the analysis of the measurement data are presented below.

2 | CHANNEL MEASUREMENT CAMPAIGN

The measurement campaign were performed in line with the concept of the future 5G indoor cellular mobile network, which employs the very directional steerable antennas at new mmWave operating frequency bands. This measurement campaign targets to explore the large-scale fading characteristics of indoor small-cell propagation channel as well as delay and angular dispersion of channel at 26 GHz, 32 GHz and 39 GHz over 2 GHz bandwidth.

2.1 | Measurement Equipment

A Rohde & Schwarz signal generator R&S®SMW200A is used to transmit continuous wave signal in power of 17 dBm. Due to its outstanding autocorrelation properties, Frank-Zadoff-Chu (FZC) sequence is employed as sounding signal which provides high autocorrelation properties. The received signal is recorded by a Rohde & Schwarz signal analyzer R&S®FSW67 to capture I/Q data, later the R&S® TS-5GCS software tool processes received data which enables us to perform channel sounding measurement. FSW and SMW are connected with two cables to be synchronized by a reference frequency, and the measurement is started by a trigger signal. To support bandwidths up to 2 GHz, an R&S®RTO1044 oscilloscope is provided to operate with the FSW. The oscilloscope offers a wide bandwidth D/A conversion. In addition, antenna rotator table, which is connected to the control machine by the fiber optic cables, enables azimuth scanning at the receiver (RX) with a rotation increment step of 5° and 8°. As shown in Fig. 1, a computer (PC) is used to not only control the antenna rotator table, but also control the FSW using the LAN cables.

2.2 | Transmitter and Receiver Antennas

Wideband and directional lens antenna is used at the RX with the same gain in both E- and H-plane of 24 dBi at 26 GHz with half power beam width (HPBM) of 5° in both planes, which is narrow enough to obtain directional channel impulse responses (CIRs) with high resolution in azimuth of arrival and delay. At transmitter (TX) side, quasi-

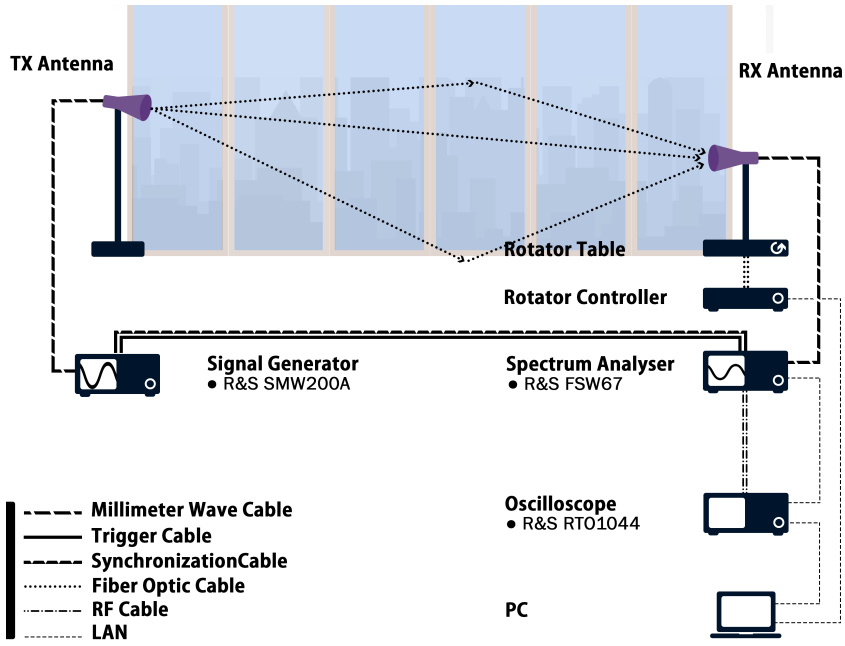

FIGURE 1 Automatic mmWave channel measurement setup.

directional pyramid horn antenna with 61° HPBM is used in the channel measurements with gain of 6.8 dBi at 26 GHz. To measure CIRs at 32 GHz and 39 GHz, wideband and directional horn antenna operating from 26.5 GHz to 40GHz is used as RX with with HPBM of 8°, while at TX side, quasi-directional horn antenna with HPBM of 54° was used in the channel measurements with gain of 10 dBi and bandwidth of 13.5 GHz from 26.5 GHz to 40 GHz. Before starting the channel measurements, the SMW was directly connected to the FSW to take calibration data. V-V, and V-H antenna polarizations (co- and cross- polarization) are conducted which the first symbol refers to the TX antenna polarization and the latter to the RX antenna polarization. Specification of the TX and RX antennas and hardware along with measurement equipment and setup are provided in Table 1.

2.3 | Measurement Environments

Measurements were conducted in the ground floor of 5G innovation center (5GIC), University of Surrey, U.K. The ground floor is a typical office environment with common obstructions such as desks, chairs, offices, doors, elevator, walls made of drywall and glass. Fig. 2 displays the detailed layout and the measuring arrangement of the measurement environment. TX antenna is placed 2.7 m above the floor to emulate common indoor hotspot locations, and RX antenna is placed 1.6 m above the floor, which is typical handset level heights. The TX antenna is fixed, while the RX antenna moves along a circular route for all the 26 GHz, 32 GHz, and 39 GHz measurements with both co- and cross- polarization antenna configurations. In each point of measurement, 32- and 39 GHz RX antenna was rotated in azimuth in small steps of 8° without changing the elevation setting whilst 26 GHz TX antenna was rotated with 5° precision in the azimuth plane. The separation distance between TX and RX for all three frequencies was ranged between 4 to 20 m with adjacent separation of 2 m and measurement points were kept fixed for the fair comparison.

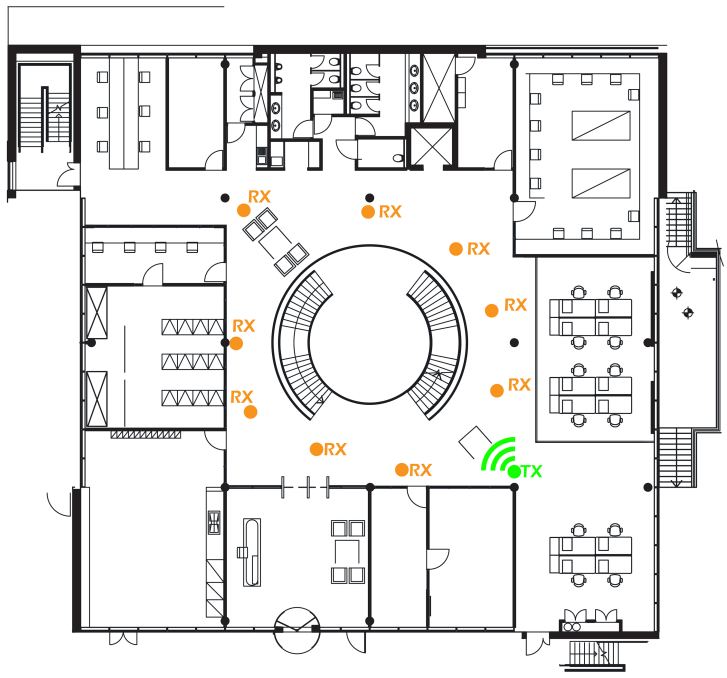

FIGURE 2 Map of the ground plan of 5GIC with TX and RX locations.

During the measurements, there was no human activity in the measurement environment, so the channel is considered as a time-invariant channel.Fig.3 shows the measurement environment along with TX and RX equipment.

3 | MEASUREMENT RESULTS, ANALYSIS, AND DISCUSSION

The measured channel impulse responses for both polarization configuration and different frequencies are derived with a delay resolution of 0.5 ns and azimuth angle of arrival resolution of 5° for 26 GHz and 8° for 32 GHz and 39 GHz. To filter out the small scale fading of each single CIR, measured CIRs are averaged over each direction on the azimuth at each measurement point to form a power delay profile (PDP). To simplify the characterization of the channel power dispersion, a set of parameters can be extracted from the PDP. In this section, power angular spectrum for V-V polarization at all frequencies is presented for comparison between 26 GHz, 32 GHz, and 39 GHz. In addition, all RMS delay spread and temporal statistics for different polarization and frequencies are presented and discussed. Large-scale fading characteristics are also studied and discussed.

3.1 | Power angular spectrum

The angular dispersion can be expressed with the power angular spectrum (PAS), which characterizes how the signal power varies over an angle. Fig. 4 shows the directional received power versus angle of arrival at each measurement

(a) (b)

FIGURE 3 (a) Transmitter and receiver equipments at 32 GHz, (b) directional lens antenna operating at 26 GHz along with the R&S®FSW67 and R&S®RTO1044 oscilloscope.

point to present the angular dispersion at (a) 26 GHz,(b) 32 GHz, and (c) 39 GHz for V-V antenna polarization. From Fig. 3 (a), it is observed that not only LoS components are strong which are shown at ($\theta = 0°$), but also, there are other strong components at other azimuth angle of arrival referring to the reflections when RX antenna was rotated toward the specific clusters in the measurement environment such as glass walls. Same behaviour has been observed at 32 GHz and 39 GHz, as well. The only difference between is the weaker received signal power value at higher frequency bands.

3.1.1 | RMS angular spread

Presented PAS in Fig. 4 with 5 ° and 8 ° angular resolution is fine enough to give a useful indication of the angular spread, but RMS Angular spread is another parameter that is useful for the successful design of MIMO and smart antenna systems [4] which can be estimated from the obtained data with the highly directional antennas at the RX.

$$\theta_{\text{rms}} = \sqrt{\frac{\sum_i P(\theta_i)(\theta_i - \theta_{\text{mean}})^2}{\sum_i P(\theta_i)}} \tag{1}$$

where, $P(\theta_i)$ is the received power at angle θ_i, and θ_{mean} is the mean azimuth angle of arrival. Fig. 5 presents the RMS angular spread for 26, 32 and 39 GHz for V-V antenna polarisation configuration. From this figure, it is observed that higher frequency bands have lower RMS angular spread.

TABLE 1 Wideband Channel Sounding Setup Specifications and antenna parameters for the 26 GHz, 32 GHz, and 39 GHz.

Frequencies	26 GHz	32 GHz	39 GHz
Sounding Waveform	Frank-Zadoff-Chu 65535		
RF Bandwidth	2 GHz		
Transmitted Power	17 dBm		
Delay Resolution	0.5 ns		
TX Polarization	Vertical		
RX Polarization	Vertical / Horizontal		
TX E-Plane Beam width	78°	54°	
TX H-Plane Beam width	61°	54°	
RX E-Plane Beam width	5°	8°	
RX H-Plane Beam width	5°	8°	
Height of TX Antenna (h_T)	2.7 m		
Height of RX Antenna	1.6 m		
TX Antenna Gain	6.8 dBi	10 dBi	
RX Antenna Gain	24 dBi	23 dBi	25 dBi

TX, transmitter; RX, receiver.

3.2 | RMS delay spread

Analogous to the RMS angular spread, the delay dispersion can be described by root mean square (RMS) delay spread which is defined as the square root of the second moment of a PDP:

$$\tau_{\text{rms}} = \sqrt{\frac{\sum_i P_i(\tau_i - \tau_{\text{mean}})^2}{\sum_i P_i}} \tag{2}$$

where, τ_{i} is the delay of the i_{th} multipath with received power of P_{i}, and τ_{mean} is the average delay of the multipath. It must be noted that RMS delay spread is a good measure of the multipath time dispersion and coherence bandwidth nature of multipath channels. It was recently expressed that there should be some advantages to search particular beam pointing directions which offer both minimum multipath delay spread and minimum path loss which can enable physical layer designers to build power-efficient mmWave mobile communication systems with simple equalization. Fig. 6 shows the cumulative distribution function (CDF) for the RMS delay spreads of the PDPs measured over all pointing angles at 26 GHz, 32 GHz, and 39 GHz for V-V and V-H antenna polarization. The RMS delay spread values are calculated using Eq. (1). In Eq. (1) a threshold of S dB below the maximum peak must be applied to the individual values of the averaged PDP to distinguish the multipath components from the noise [8]. It must be noted that the value of S, directly affects the value of τ_{rms}. Commonly used values of S which can be found in literature include 15, 20 , and 30 dB below the maximal which set the threshold 5 - 30 dB above the noise floor depending on the measurement position. In this paper all RMS delay spread values for V-V antenna polarization is calculated by considering only paths that exceeded a 35 dB threshold below the maximum peak (S = 35 dB) in the PDPs to have a wide dynamic range and

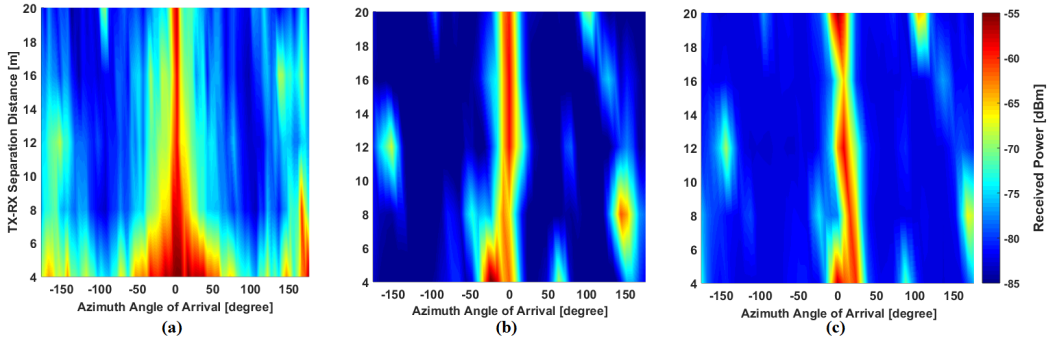

FIGURE 4 Absolute directional received power at (a) 26 GHz, (b) 32 GHz, and (c) 39 GHz.

TABLE 2 RMS delay spread for the 26 GHz, 32 GHz, and 39 GHz for different antenna polarization configuration.

Carrier Frequency [GHz]	26		32		39	
Polarization	V-V	V-H	V-V	V-H	V-V	V-H
RMS delay spread [ns]	26.78	5.88	24.27	3.57	20.48	2.72

fair comparison between three different frequency bands as their noise floors have different values. In this case, the 90% of the measured RMS delay spreads of V-V configuration are less than 26.78 ns, 24.27 ns, and 20.48 ns at 26 GHz, 32 GHz, 39 GHz, respectively which is apparent that 90% of the energy arrived at the RX is less than 27 ns at 26 GHz for all measured arbitrary pointing angles. To calculate RMS delay spreads for V-H antenna polarization, 20 dB threshold has been applied due to short dynamic range in this case, and as it is expected their values are small for H-V antenna polarization at all frequency bands. 5.88 ns, 3.57 ns, and 2.72 ns were calculated for 26 GHz, 32 GHz, and 39 GHz, respectively which are much more less than V-V cases because cross-polarized signal components are generated by depolarized multipath due to reflection and diffraction. As it can be seen that from Fig. 6, the RMS delay spread at 39 GHz is smaller than at 26 GHz, and 32 GHz for each polarization similar to results reported in [31] when comparing RMS delay spreads of 28 GHz, 38 GHz, and 73 GHz. This difference is due to the greater energy being scattered at lower mmWave frequencies. On the other hand, wavelengths at 39 GHz are smaller than at 26 GHz and 32 GHz which cause to more diffuse scattering during propagation which results in weaker path which are not detectable in the receiver. To better understanding of this phenomena, Fig. 7 is presented to show the omni-directional received power at each measurement point versus delay values for different type of polarization at 26 GHz, 32 GHz, and 39 GHz, which can clearly show more dispersion at 26 GHz compared to 32 GHz and 39 GHz shows how signal have been scattered in three different bands. The reason is, there are more resolvable multipath component as a function of TX-RX separation at 26 GHz compared to 32 GHz and 39 GHz due to stronger signals and larger wavelenghts at 26 GHz, which allow the signal to reflect more and scatter less. RMS delay spread values for different frequencies and polarisations are listed in Table 2.

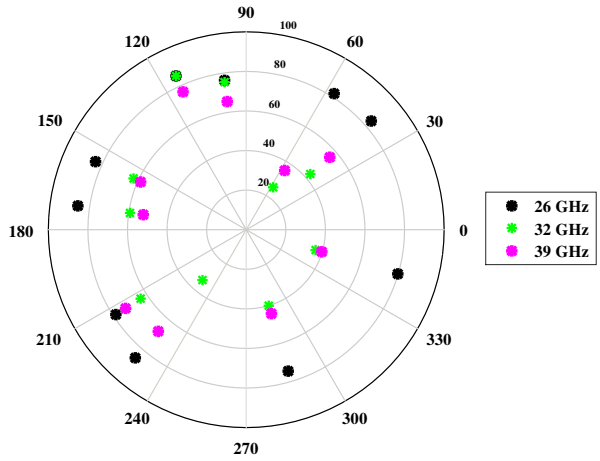

FIGURE 5 RMS angular spread for 26 GHz, 32 GHz, and 39 GHz for V-V polarisation configuration.

3.3 | Path loss

The path loss (PL) is the main parameter to describe the large-scale characteristics of the channel. Attenuation over distance can be estimated by PL models, which are vital for designing wireless communication systems and were investigated based on deterministic, empirical, and stochastic PL models while, the most realistic PL models is based on measurements. The PL can be given by:

$$L(d) = P_t + G_t + G_r - P_r(d) - L_0[\text{dB}] \tag{3}$$

In (3), G_t and G_r respectively denote TX and RX antenna gains in dBi, and P_t and P_r respectively represent transmitted power and received power in dBm, and L_0 is mmWave cable loss in dB.

3.3.1 | CI PATH LOSS MODEL

One of the most popular PL models is single frequency path loss model (CI model), defined as

$$\text{PL}^{\text{CI}}(f, d)[\text{dB}] = \text{FSPL}(f, d_0) + 10n \log_{10}(d/d_0) + X_\sigma^{\text{CI}} \tag{4}$$

where $\text{PL}^{\text{CI}}(f, d)$ represents the path loss at a given frequency of f with different TX-RX separation distance of d, whilst $\text{FSPL}(f, d_0)$ is the path loss in dB at a close-in (CI) distance d_0. Moreover, X_σ is a zero mean Gaussian random variable with standard deviation of σ in dB. The CI model is based on determining the path loss exponent (PLE) n using the minimum mean square error (MMSE) method in order to fit the measured data with smallest error

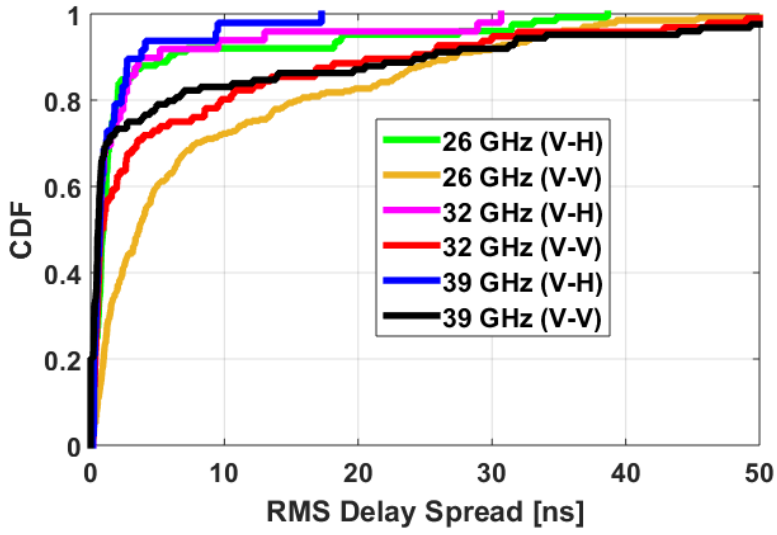

FIGURE 6 26 GHz, 32 GHz, and 39 GHz RMS delay spread CDFs for different antenna polarization configuration.

TABLE 3 Large-scale fading parameters for the 26 GHz, 32 GHz, and 39 GHz.

Carrier Frequency [GHz]	26		32		39	
Polarization	V-V	V-H	V-V	V-H	V-V	V-H
Path Loss Component (n)	1.68	2.87	1.88	2.99	1.81	2.93
σ	2.9	4.3	2.5	4.1	2.2	3.8

through minimizing σ and using a true physically-based reference distance of d_0. The CI path loss model is therefore employed by considering d_0 = 1m as a reference point. LSF characteristics including the PLE and standard deviation of the resulting shadow fading σ from the channel measurement data, provided in Table 3 for 3 frequencies and both co- and cross- polarization. For V-V antenna polarization, the PLEs are 1.68, 1.88, and 1.81 at 26 GHz, 32 GHz, and 39 GHz, respectively. These results show that the PLE values for the three frequencies in indoor environment are less than but very close to the theoretical free space path loss component (n = 2). These results indicate that the multipath components from different reflectors in the office environment add up constructively as a waveguide effect and showing that directional LoS PLEs are independent of frequency. The PLEs are 4.3, 4.1, and 3.8 at 26 GHz, 32 GHz, and 39 GHz, respectively for V-H antenna polarization.

3.3.2 | 3GPP Indoor Path Loss Model

3GPP defined the path loss model for LoS scenarios in the indoor-office environment as

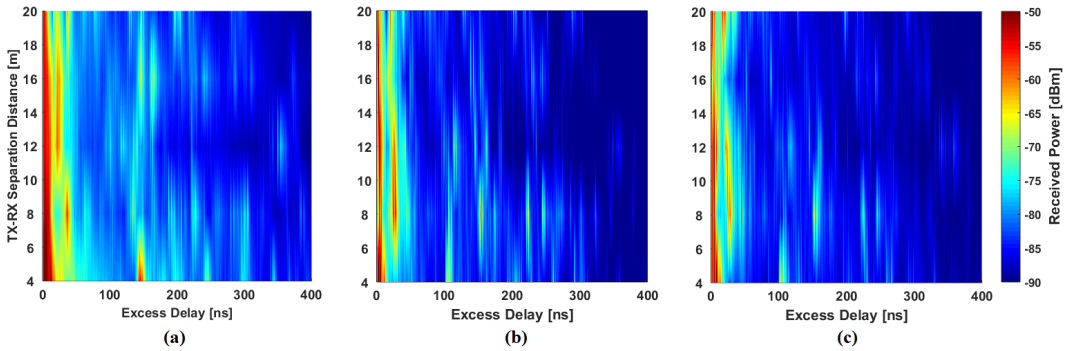

FIGURE 7 Omni-directional power delay profile for the (a) 26 GHz (V-V), 32 GHz (V-V), and 39 GHz (V-V).

$$\mathrm{PL}_{\text{InH-LoS}} = 32.4 + 17.3 \log_{10}(d_{3D}) + 20 \log_{10}(f_c) \tag{5}$$

In (5), f_c is the center frequency in GHz, d_{3D} is the 3-dimensional distances between TX and RX antennas in meter, respectively. This model is valid for d_{3D} from 1 to 100 meter with shadow fading of σ_{SF} = 3 while Table 3 shows the maximum shadow fading of 2.9 for 26 GHz when both TX and RX antenna are in same polarization.

4 | CONCLUSION

Indoor wideband directional channel measurements were conducted to obtain large-scale characteristics at 26 GHz, 32 GHz, and 39 GHz bands for LoS scenario. The delay resolution was 0.5 ns while high gain directional antenna at transmitter side, and mechanically steerable highly directional antenna at receiver side have been used. Measurements were performed on 5GIC ground floor, University of Surrey, which include different type of obstructions. Channel characteristics such as power angular spectrum as well as RMS delay spread are presented and discussed. It is found that LoS components are dominant and there are other strong specular reflections in the receiver from other directions in these bands and scenarios. The RMS delay spread of the directional received signal shows a small delay spread around the dominant received signal components. Also, RMS angular spread was presented for different frequencies where, higher bands have lower values. In addition, CI path-loss model has been studied and shown that for the co-polarized channel (V-V scenario), constructive interference due to waveguiding and reflections resulted in the PLEs to be less than theoretical free space path loss component (n = 2). PLEs for V-H polarisation configuration are greater than 2 due to significant de-polarization effect. 3GPP indoor path loss model was studied and compared with the measured path loss at 26, 32, and 39 GHz.

Acknowledgments

We would like to acknowledge the support of the University of Surrey 5GIC (http://www.surrey.ac.uk/5gic) members for this work. Also authors would like to thank Rohde and Schwarz to support this channel measurement campaign.

references

[1] AlAbdullah AA, Ali N, Obeidat H, Abd-Alhmeed RA, Jones S. Indoor millimetre-wave propagation channel simulations at 28, 39, 60 and 73 GHz for 5G wireless networks 2017 Sept;p. 235–239.

[2] Bensebti M, Mcgeehan JP, Beach MA. Indoor Multipath Radio Propagation Measurements and Characterisation at 60 GHz 1991 Sept;2:1217–1222.

[3] Chen WC, Kuo FY. ITRI mmWAVE access technology development 2016 Aug;p. 1–5.

[4] Czink N, Bonek E, Yin X, Fleury B. Cluster Angular Spreads in a MIMO Indoor Propagation Environment 2005 Sept;1:664–668.

[5] Elrefaie AF, Shakouri M. Propagation measurements at 28 GHz for coverage evaluation of local multipoint distribution service 1997 Aug;p. 12–17.

[6] Federal Communications Commission, FCC Takes Steps To Facilitate Mobile Broadband And Next Generation Wireless Technologies In Spectrum Above 24 GHz; Jul 2016. https://www.fcc.gov/document/fcc-adopts-rules-facilitate-next-generation-wireless-technologies.

[7] Geng S, Kivinen J, Zhao X, Vainikainen P. Millimeter-Wave Propagation Channel Characterization for Short-Range Wireless Communications. IEEE Transactions on Vehicular Technology 2009 Jan;58(1):3–13.

[8] Ghassemzadeh SS, Jana R, Rice CW, Turin W, Tarokh V. Measurement and modeling of an ultra-wide bandwidth indoor channel. IEEE Transactions on Communications 2004 Oct;52(10):1786–1796.

[9] Haneda K, Järveläinen J, Karttunen A, Kyrö M, Putkonen J. Indoor short-range radio propagation measurements at 60 and 70 GHz 2014 April;p. 634–638.

[10] http://www gsmhistory com/, Short history of the 5g pioneer bands; 16 January 2018. http://www.gsmhistory.com/short-history-of-the-5g-pioneer-bands/.

[11] Khalily M, Ghoraishi M, Taheri S, Payami S, Tafazolli R. Millimeter-Wave Directional Path Loss Models in the 26 GHz, 32 GHz, and 39 GHz Bands for Small Cell 5G Cellular System 2018 April;.

[12] Khalily M, Ghoraishi M, Taheri S, Payami S, Tafazolli R. Polarimetric Wideband Directional Channel Measurement and Analysis for Outdoor Small Cell Scenarios at 32 GHz and 39 GHz 2018 April;.

[13] Khalily M, Taheri S, Xiao P, Entezami F, Hill TA, Tafazolli R. 26 GHz Indoor Wideband Directional Channel Measurement and Analysis in 2018 April;.

[14] Kim MD, Liang J, Kwon HK, Lee J. Directional delay spread characteristics based on indoor channel measurements at 28GHz 2015 Aug;p. 403–407.

[15] Kim MD, Liang J, Lee J, Park J, Park B. Path loss measurements and modeling for indoor office scenario at 28 and 38 GHz 2016 Oct;p. 64–65.

[16] Ko J, Cho YJ, Hur S, Kim T, Park J, Molisch AF, et al. Millimeter-Wave Channel Measurements and Analysis for Statistical Spatial Channel Model in In-Building and Urban Environments at 28 GHz. IEEE Transactions on Wireless Communications 2017 Sept;16(9):5853–5868.

[17] Koymen OH, Partyka A, Subramanian S, Li J. Indoor mm-Wave Channel Measurements: Comparative Study of 2.9 GHz and 29 GHz 2015 Dec;p. 1–6.

[18] Kyro M, Kolmonen VM, Vainikainen P. Experimental Propagation Channel Characterization of mm-Wave Radio Links in Urban Scenarios. IEEE Antennas and Wireless Propagation Letters 2012;11:865–868.

[19] Lee J, Liang J, Park JJ, Kim MD. Directional path loss characteristics of large indoor environments with 28 GHz measurements 2015 Aug;p. 2204–2208.

[20] Li S, Liu Y, Chen Z, Sun X, Lin L. Measurements and modelling of millimeter-wave channel at 28 GHz in the indoor complex environment for 5G radio systems 2017 Oct;p. 1–6.

[21] Maccartney GR, Rappaport TS, Sun S, Deng S. Indoor Office Wideband Millimeter-Wave Propagation Measurements and Channel Models at 28 and 73 GHz for Ultra-Dense 5G Wireless Networks. IEEE Access 2015;3:2388–2424.

[22] METIS, Deliverable D1.4 METIS channel models; Feb. 2015. www.metis2020.com/documents/deliverables. Deliverable ICT-317669-METIS/D1.4.

[23] MiWEBA, D1.1: Definition of scenarios and use cases; Dec. 2013. www.miweba.eu/#Publications. Deliverable FP7-ICT 608636/D1.1.

[24] mmMagic, 6-100 GHz channel modelling for 5G: Measurement and modelling plans in mmMAGIC; Feb. 2016. bscw.5g-mmmagic.eu/pub/bscw.cgi/d76988/mmMAGIC_WhitePaper-W2.1.pdf.

[25] Molu MM, Xiao P, Khalily M, Cumanan K, Zhang L, Tafazolli R. Low-Complexity and Robust Hybrid Beamforming Design for Multi-Antenna Communication Systems. IEEE Transactions on Wireless Communications 2018 March;17(3):1445–1459.

[26] Ofcom, Ofcom Notes: Update on 5G spectrum in the UK; 8 February 2017. https://www.ofcom.org.uk/__data/assets/pdf_file/0021/97023/5G-update-08022017.pdf.

[27] Payami S, Ghoraishi M, Dianati M. Hybrid Beamforming for Large Antenna Arrays With Phase Shifter Selection. IEEE Transactions on Wireless Communications 2016 Nov;15(11):7258–7271.

[28] Payami S, Ghoraishi M, Dianati M, Sellathurai M. Hybrid Beamforming with Reduced Number of Phase Shifters for Massive MIMO Systems. IEEE Transactions on Vehicular Technology 2018;PP(99):1–1.

[29] Pi Z, Khan F. An introduction to millimeter-wave mobile broadband systems. IEEE Communications Magazine 2011 June;49(6):101–107.

[30] Raghavan V, Partyka A, Sampath A, Subramanian S, Koymen OH, Ravid K, et al. Millimeter-Wave MIMO Prototype: Measurements and Experimental Results. IEEE Communications Magazine 2018 Jan;56(1):202–209.

[31] Rappaport TS, MacCartney GR, Samimi MK, Sun S. Wideband Millimeter-Wave Propagation Measurements and Channel Models for Future Wireless Communication System Design. IEEE Transactions on Communications 2015 Sept;63(9):3029–3056.

[32] Rappaport TS, Sun S, Mayzus R, Zhao H, Azar Y, Wang K, et al. Millimeter Wave Mobile Communications for 5G Cellular: It Will Work! IEEE Access 2013;1:335–349.

[33] Roh W, Seol JY, Park J, Lee B, Lee J, Kim Y, et al. Millimeter-wave beamforming as an enabling technology for 5G cellular communications: theoretical feasibility and prototype results. IEEE Communications Magazine 2014 February;52(2):106–113.

[34] Sasaki M, Inomata M, Yamada W, Kita N, Onizawa T, Nakatsugawa M, et al. Path loss characteristics between different floors from 0.8 to 37 GHz in indoor office environments 2016 Oct;p. 66–67.

[35] Wang M, Liu Y, Li S, Chen Z. 60 GHz millimeter-wave propagation characteristics in indoor environment 2017 May;p. 749–752.

[36] Wang Q, Li S, Zhao X, Wang M, Sun S. Wideband Millimeter-Wave Channel Characterization Based on LOS Measurements in an Open Office at 26GHz 2016 May;p. 1–5.

[37] Wu X, Zhang Y, Wang CX, Goussetis G, e H M Aggoune, Alwakeel MM. 28 GHz indoor channel measurements and modelling in laboratory environment using directional antennas 2015 May;p. 1–5.

[38] Xu H, Kukshya V, Rappaport TS. Spatial and temporal characterization of 60 GHz indoor channels 2000;1:6–13 vol.1.

[39] Zhao H, Mayzus R, Sun S, Samimi M, Schulz JK, Azar Y, et al. 28 GHz millimeter wave cellular communication measurements for reflection and penetration loss in and around buildings in New York city 2013 June;p. 5163–5167.

[40] Zhao X, Li S, Wang Q, Wang M, Sun S, Hong W. Channel Measurements, Modeling, Simulation and Validation at 32 GHz in Outdoor Microcells for 5G Radio Systems. IEEE Access 2017;5:1062–1072.

[41] Zhu J, Wang H, Hong W. Large-Scale Fading Characteristics of Indoor Channel at 45-GHz Band. IEEE Antennas and Wireless Propagation Letters 2015;14:735–738.

[42] Zwick T, Beukema TJ, Nam H. Wideband channel sounder with measurements and model for the 60 GHz indoor radio channel. IEEE Transactions on Vehicular Technology 2005 July;54(4):1266–1277.